energies

MDPI

Article

High Performance Electric Vehicle Powertrain Modeling, Simulation and Validation

Feyijimi Adegbohun [1], Annette von Jouanne [1,*], Ben Phillips [2], Emmanuel Agamloh [1] and Alex Yokochi [2]

[1] Department of Electrical and Computer Engineering, Baylor University, Waco, TX 76798, USA; jimi_adegbohun@baylor.edu (F.A.); Emmanuel_Agamloh@baylor.edu (E.A.)
[2] Department of Mechanical Engineering, Baylor University, Waco, TX 76798, USA; ben_phillips@baylor.edu (B.P.); Alex_Yokochi@baylor.edu (A.Y.)
* Correspondence: annette_vonjouanne@baylor.edu

Abstract: Accurate electric vehicle (EV) powertrain modeling, simulation and validation is paramount for critical design and control decisions in high performance vehicle designs. Described in this paper is a methodology for the design and development of EV powertrain through modeling, simulation and validation on a real-world vehicle system with detailed analysis of the results. Although simulation of EV powertrains in software simulation environments plays a significant role in the design and development of EVs, validating these models on the real-world vehicle systems plays an equally important role in improving the overall vehicle reliability, safety and performance. This modeling approach leverages the use of MATLAB/Simulink software for the modeling and simulation of an EV powertrain, augmented by simultaneously validating the modeling results on a real-world vehicle which is performance tested on a chassis dynamometer. The combination of these modeling techniques and real-world validation demonstrates a methodology for a cost effective means of rapidly developing and validating high performance EV powertrains, filling the literature gaps in how these modeling methodologies can be carried out in a research framework.

Keywords: electric vehicle; chassis dynamometer; drive cycle; modeling

Citation: Adegbohun, F.; von Jouanne, A.; Phillips, B.; Agamloh, E.; Yokochi, A. High Performance Electric Vehicle Powertrain Modeling, Simulation and Validation. *Energies* **2021**, *14*, 1493. https://doi.org/10.3390/en14051493

Academic Editor: Hrvoje Pandzic

Received: 16 February 2021
Accepted: 1 March 2021
Published: 9 March 2021

1. Introduction

The electric vehicle (EV) market continues to grow, with over seven million EVs on the road worldwide [1]. The International Energy Agency (IEA) forecasts that these numbers will exceed 125 million by 2030 [2]. EVs offer increased efficiency and energy savings, reduced emissions (especially when the electricity is being generated from renewable resources), higher performance and a greater diversity of fuel choices for transportation. For these reasons, the world is also seeing an increased trend in high performance EVs, and in converting traditional internal combustion engine (ICE) vehicles to EVs. The goals of high performance EVs include addressing the challenges of cost, range anxiety, charging time and infrastructure, battery state of health, and impacts of vehicle to grid (V2G) operations, while increasing transportation safety [3]. According to the U.S. Department of Transportation (DoT), 94% of all serious car accidents occur due to human error [4]. Thus, the opportunities that high performance EVs provide for increased levels of autonomous EV operation further enable increased transportation safety, while also adding levels of convenience and independence for the world's aging population [5].

Understanding the operation of the EV under a variety of driving and environmental conditions is critical to optimizing vehicle performance, vehicle health and vehicle safety. Some of the conditions that could affect vehicle performance such as temperature, road conditions, road grade/elevation, aggressive/conservative driving, etc. need to be validated for vehicle reliability and performance estimation [6]. To estimate these metrics and make the critical design and control decisions needed during vehicle design and vehicle validation, the EV powertrain must be modeled accurately, and simulated and analyzed in

a scalable fashion [7–10]. Furthermore, these models must be flexible and robust enough to be tuned based on the real-world data to provide improved vehicle serviceability once the vehicle is in the field.

Vehicle modeling occurs in different forms, such as mathematical models, steady state models, multi-physics domain physical modeling, dynamics and transient modeling [11], with significant advancements in recent years. Vehicle modeling can also occur at different levels of fidelity and precision, such as system level modeling, component modeling or sub-system level modeling. The selection of the model type and modeling tools is indicative of the kinds of questions that the model is expected to answer and the forms of analyses that are intended to be performed on the modeling results. However, the reliance on simulation-based platforms alone for the validation of vehicle models is insufficient, and the development and testing of vehicle prototypes for public road testing could be unsafe, impractical and sometimes very costly. Therefore, a balance between simulation and some level of real-world testing in a scalable fashion is necessary in the development of high performance EV powertrains.

MATLAB/Simulink software is a tool capable of modeling complete EV powertrains of different levels of fidelity and detail and has become an invaluable modeling platform. This software features a variety of shipped sample models for simulation of pure battery electric as well as hybrid electric vehicles of different configurations and types [12–15]. The MATLAB/Simulink platform supports many add-ons which have been used in vehicle modeling, such as SimPowerSystems and SimDriveline [15], Advisor [13], Simscape, Powertrain Blockset, etc. Simulink supports an equation-based modeling approach, a data-driven modeling approach, as well as a physical modeling approach for vehicle modeling. Simulink also supports code generation for hardware testing and deployment, testing and analysis frameworks for test case management and report generation. MATLAB/Simulink models have been widely studied in the literature [10–15], however, methodologies for validating these models within the real-world environment in a research setting has not been addressed adequately in existing literature.

In this paper, the authors describe the modeling and simulation steps for high performance EVs by defining key vehicle specifications and then developing an equation-based model of a battery EV in MATLAB/Simulink software. The modeling goal is to test for the efficiency and performance of the EV and the results of the model are validated by real-world tests on the target EV platform. In Section 2, a summary of vehicle motion dynamics is presented and the modeling methodology is described where a generic equation-based model that ships with the MATLAB/Simulink software [16] is significantly modified based on the specifications and initial testing conducted on the target vehicle platform. In Section 3, the procedure and the detailed results of the chassis dynamometer performance testing conducted on the modeled vehicle is described. Section 4 presents the results of the model and detailed analysis. Section 5 concludes the paper including the primary findings and statistical results.

2. Equation-Based Modeling Summary

For equation-based modeling, the dynamics of vehicle motion represented in drive cycles and the vehicle systems must be formulated and then implemented in the form of subsystems, blocks and signals within Simulink. The next sections summarize the equations that govern vehicle motion and vehicle systems needed for modeling.

2.1. Dynamics of Vehicle Motion

Newton's second law states that the acceleration of an object is proportional to the net force exerted on it. In other words, an object accelerates when the net force exerted on it is nonzero. Similarly, a vehicle moves due the force of the propulsion unit (the powertrain) overcoming the gravitational force of the vehicle exerted on the roadway, the air resistance and the tire rolling resistance. The acceleration and speed at which the vehicle moves are dependent on the power delivered to the wheel by the powertrain, the curb mass

of the vehicle (including all of the components and passengers on board), the condition of the roadway and the aerodynamics of the vehicle on the roadway. When a vehicle is accelerating, the vehicle is subject to the forces described in Equation (1) [17]:

$$k_m m \frac{dv_{xT}}{dt} = F_{TR} - F_{RL} \tag{1}$$

where F_{TR} represents the tractive force which the electric machine delivers, F_{RL} represents road load forces, m represents vehicle mass, v_{xT} is the velocity in the tangential direction of the roadway, k_m accounts for the rotational inertia coefficient of the onboard vehicle's rotating mass, and $k_m m \frac{dv_{xT}}{dt}$ ccounts for forces that propel the vehicle forward. F_{RL} is the summation of the gravitational force F_{gxT} acting on the vehicle in the downward direction, rolling resistance of the vehicles tires F_{roll}, and the aerodynamic drag F_{AD} as described in Equations (2)–(5) [17]:

$$F_{RL} = F_{gxT} + F_{roll} + F_{AD} \tag{2}$$

$$F_{gxT} = m \times g \times sin\beta \tag{3}$$

$$F_{roll} = m \times g \times cos\beta\left(C_o + C_1 {v_{xT}}^2\right) \text{ for } v_{xT} > 0 \tag{4}$$

$$F_{AD} = \frac{1}{2}\rho C_D A_F (v_{xT} + v_0)^2 \text{ for } v_{xT} > 0 \tag{5}$$

where C_o and C_1 are coefficients of rolling resistance, the grade in degrees is given by β, g is the acceleration due to gravity, air density is ρ, C_D is the coefficient of drag, A_F is the frontal area, and v_0 is the measured head wind velocity ahead of the vehicle. Equation (5) defines the aerodynamic force relationship to the aforementioned constants and variables. Figure 1 is referred to as a free body diagram or point mass diagram and it describes the forces that act on the EV on a roadway [18].

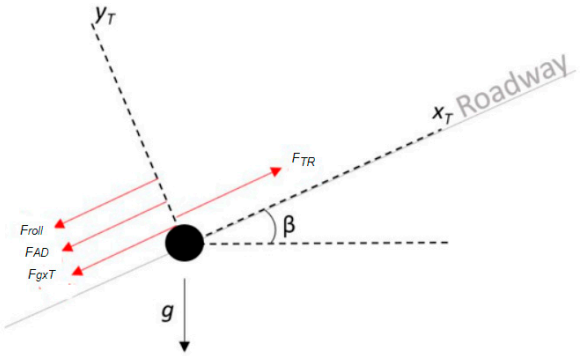

Figure 1. Free body diagram of forces acting on an EV. Adapted from [18], IEEE: 2020.

The tire-road interaction of the vehicle and the traction properties of the tire-road interface are fundamental to the dynamics of a vehicle. The traction torque from the propulsion system is converted into a traction force through the interaction between the pneumatic tire and the road surface at the tire-road interface [17] illustrated in Figure 2. The speed of tire and the longitudinal speed of the vehicle vary in magnitude and direction and are a function of the forces acting on the tire, including the vertical load force that the vehicle body exerts on the wheel, F_z, and the longitudinal forces exerted on the tire at the tire-road interface, F_x. The rolling speed of the tire is related to the tire angular velocity and wheel radius r_w and is given by Equation (6) [16]:

$$v_{tire} = r_w \Omega \tag{6}$$

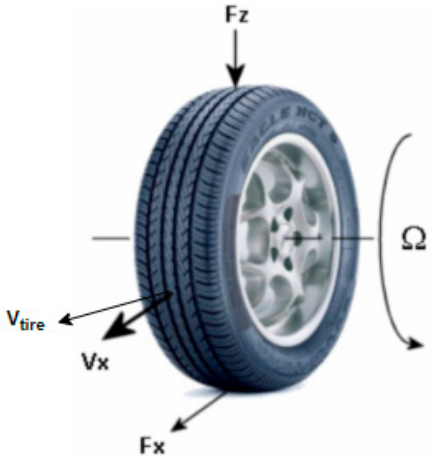

Figure 2. Speed and forces in the tire-road contact patch area. Adapted from [16], MathWorks: 2020.

The ratio of the longitudinal velocities of the vehicle V_x and the tire V_{tire}, is defined as the wheel slip s given by

$$s = 1 - \frac{V_x}{V_{tire}} \tag{7}$$

During braking, the slip of the vehicle is given by

$$s = 1 - \frac{V_{tire}}{V_x} \tag{8}$$

2.2. Drive Cycles for Modeling and Testing

In practice, the environmental protection agency (EPA) sets the standards for allowable emmisions and efficiency requirements for automakers and original equipment manufacturers (OEMs). A critical part of the design philosophy in any vehicle development program is meeting these stringent efficiency requirements. For ICE vehicles, the EPA has historically leaned on the Single Cycle Test (SCT) in determining emmisions and efficiency ratings of new vehicles and enforcing the emmision regulations. SCTs, however, are not suitable for characterizing the effects of ambient temperatures and other ancillary loads that an EV might be subject to in the real world. A new testing procedure referred to as the Multi-Cycle Test has therefore been adopted in the efficiency testing conducted by EPA which reduces the testing time for an EV by over 75%, from over 18 h to just over 4 h [19]. Given the goal of the model described in this work, which is to test the efficiency of the target EV platform, the authors have devised a shorter form of the MCT which still captures the basic principles of the tests used by the EPA. This test developed includes a combination of the US06, which is an aggressive drive cycle, and the Highway Fuel Economy Test (HWFET). The US06 cycle is an 8-mile route with an average speed of 48.4 mph, with maximum speeds of 80.3 mph and total duration of 596 s. The HWFET covers a distance of 10.26 miles, with an average speed of 48.3 mph and a duration of 765 s providing a total MCT test duration of ~22 min and 18.26 miles covered in distance. Figure 3 is a plot of the combined MCT drive cycle used in this work for efficiency test modeling and validation.

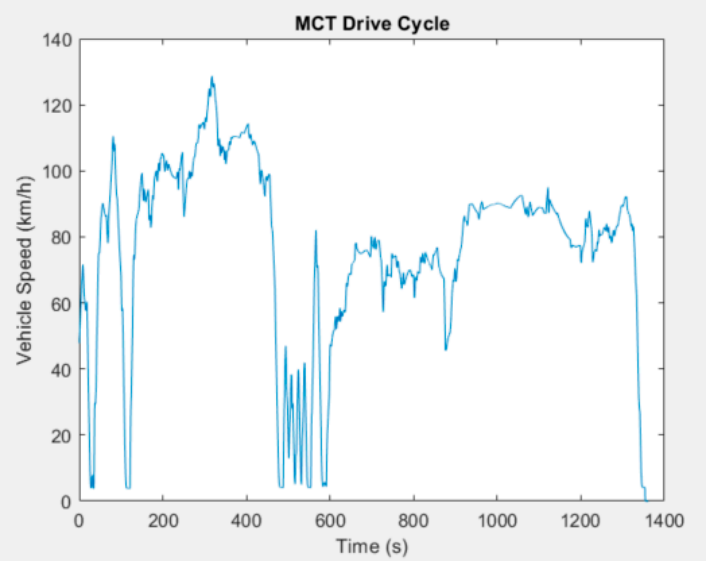

Figure 3. Multi-Cycle Test (MCT) drive cycle, reducing the testing time of EVs. The total time and distance for this MCT test was ~22 min and 18.26 miles (29.3 km).

2.3. EV Powertrain Modeling and Simulation

EV powertrain modeling and simulation begins with the determination of key design specifications as detailed in Table 1, adapted from the spec sheet of a Chevrolet Bolt EV. These specs are then used in an equation-based model of an EV using MATLAB/Simulink, and the modeling results are then validated using a real-world vehicle performance tested on a chassis dynamometer.

Table 1. Vehicle Specification for Chevrolet Bolt EV.

Description	Value
Initial Acceleration (0–60 mph)	7.5 s
Curb weight	1616.15 kg
Motor power	200 hp/150 kW
Motor torque	266 lb.ft/360 Nm
Final drive ratio	7.05:1
Energy efficiency	300 Wh/mile
Battery capacity	53 kWh
Top speed	93 mph
Aerodynamic drag coefficient	0.308

2.4. Glider Model

The equation-based modeling approach in Simulink involves the representation of each vehicle component or subsystem as a series of equation blocks connected to each other through signals that are calculated and updated at each time step. Figure 4 is an overview of the equation-based model in Simulink to meet the EV specifications previously described. The glider model represents the point mass model of the vehicle dynamics previously described. It sums up the forces acting on vehicle body represented by a point mass, as described in Equations (1)–(5). Table 2 is a summary of parameters used for the calculation of vehicle dynamics and determining the vehicle speed at each timestep. Figure 5 is a closer look at the glider model subsystem within the Simulink model where Equations (1)–(5) are implemented by taking in an input of tractive force and subtracting the summation of the road load forces to get the inertial force, which is converted into an

acceleration based on the vehicle mass and then integrated over time to form the output of the model, vehicle speed, which is then fed back to the driver control subsystem in Figure 6. Figure 7 is the energy and power analysis of glider model subsystem. Figure 8 is a block diagram which represents the calculations for determining values such as distance, tractive energy consumed, tractive power, velocity braking energy, etc. Note that simulation block inputs are indicated with yellow and block outputs are indicated with red.

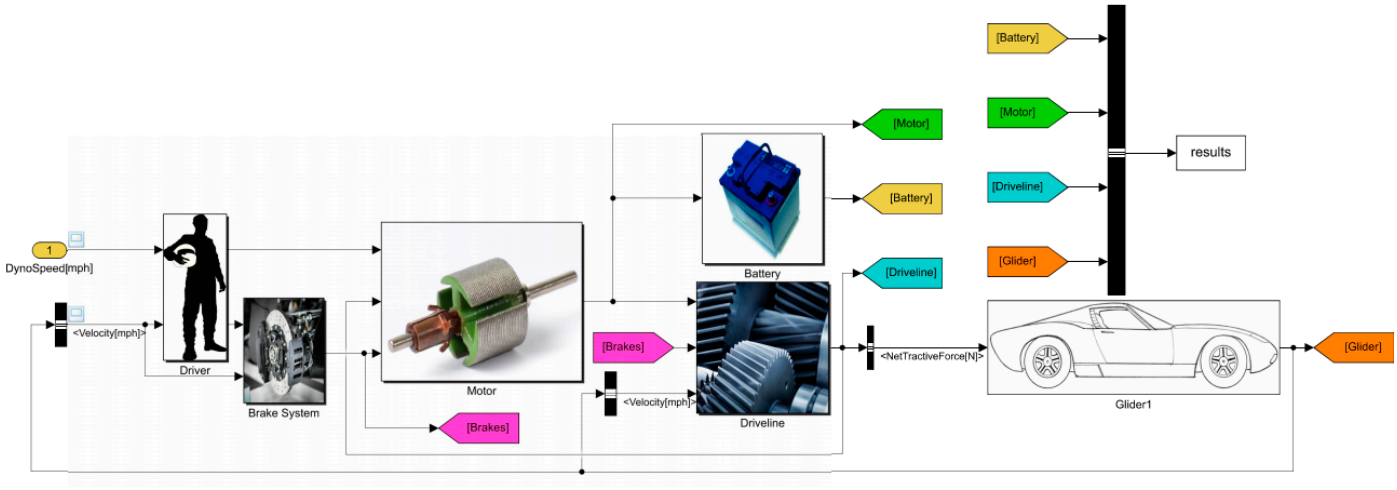

Figure 4. Simulink equation-based EV model. Adapted from [16], MathWorks: 2020.

Table 2. Glider Model Parameters Adapted from [16], MathWorks: 2020.

Parameter	Unit	Description	Value
ρ	kg/m^3	Air Density	1.23
C_d	-	Drag coefficient	0.38
A_f	m^2	Vehicle frontal Area	2.1
V	m/s	Vehicle Speed	-
a	m/s^2	Vehicle acceleration	-
m_i	kg	Vehicle inertial mass	1678.30
m	kg	Vehicle Mass	1616.15
g	m/s^2	Gravity	9.81
θ	Degrees	Road angle	0
C_{rr}	-	Rolling resistance coefficient	0.01

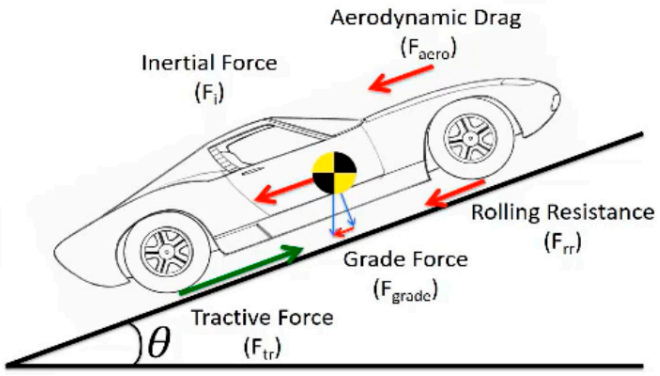

Figure 5. Vehicle body glider model Adapted from [16], MathWorks: 2020.

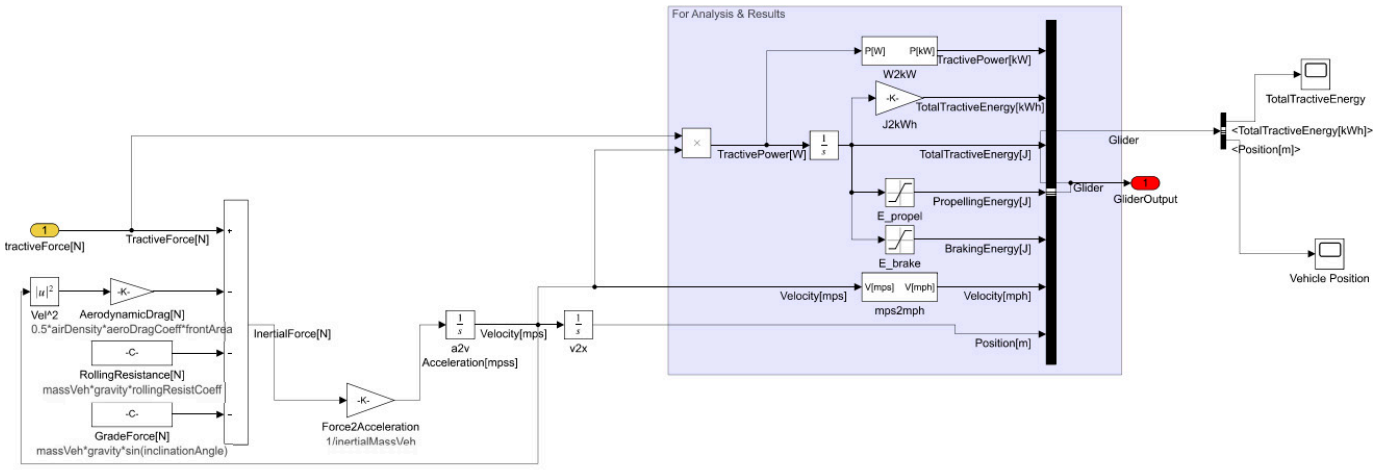

Figure 6. Vehicle glider model subsystem Adapted from [16], MathWorks: 2020.

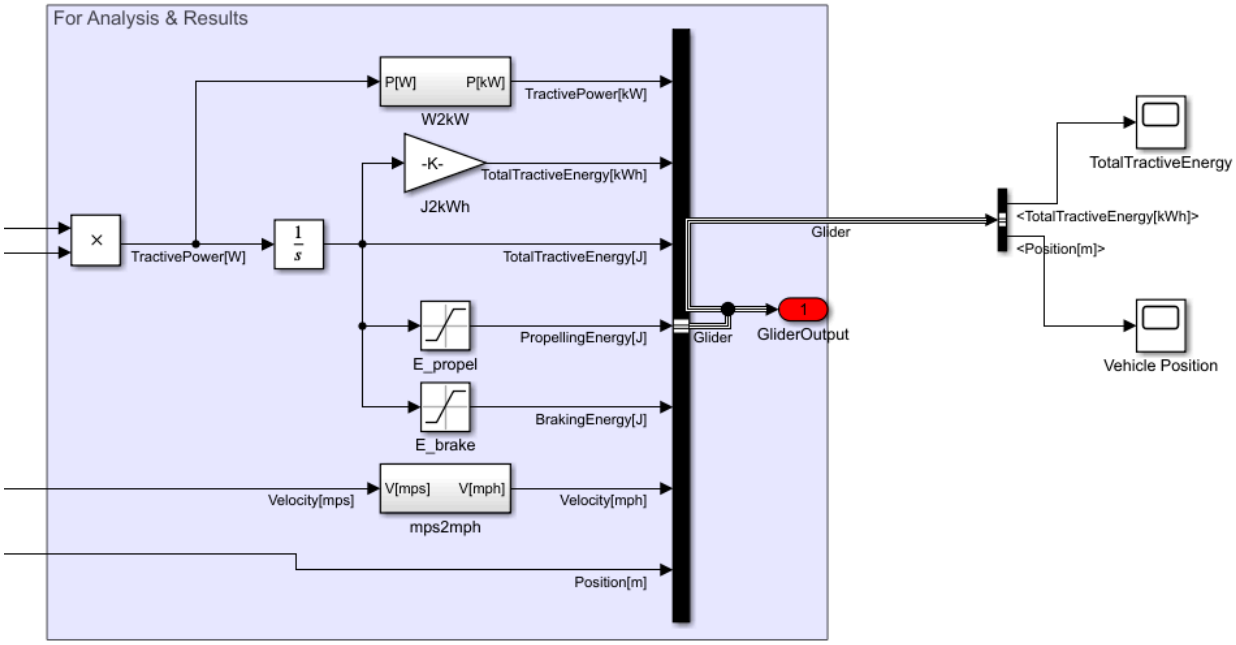

Figure 7. Energy and power analysis of the glider model subsystem Adapted from [16], MathWorks: 2020.

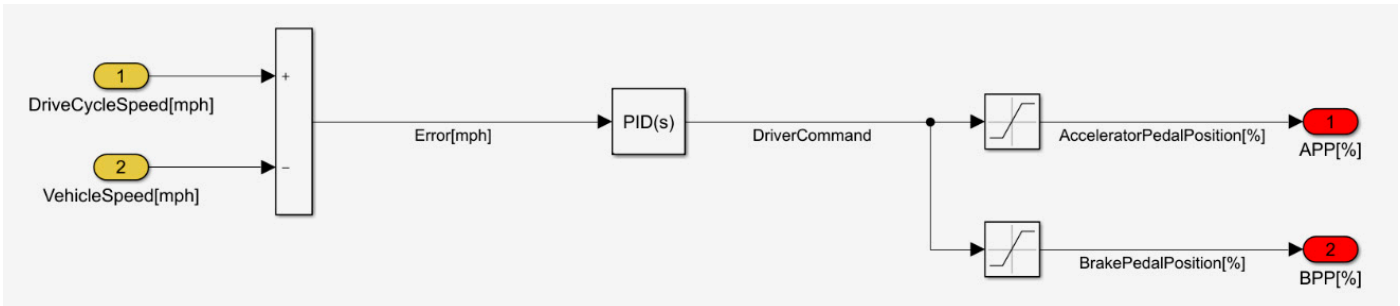

Figure 8. Driver control system block Adapted from [16], MathWorks: 2020.

2.5. Driver Model

The inputs to the driver control block are the drive cycle reference speed and the vehicle speed feedback from the glider model block. The error between the two speeds is fed back into the PID controller and the output is a driver command of either an accelerator pedal position (APP%) or a brake pedal position (BPP%).

The modeling approach of the driver subsystem mimics a real-world driver control operation, where the driver is the PID in this case and he/she observes the vehicle speed at any given time and responds with a force on either the accelerator or brake pedal to bring the vehicle to a desired speed.

2.6. Brake System

The brake system takes an input of vehicle speed and BPP%. The BPP% signal is used to determine the amount of braking force that the driver/PID is intending to apply to the vehicle and distributes this force into a regenerative braking force output and frictional brake output, based on the limitation of the motor and systems regen power. The vehicle speed input is used to determine if the vehicle speed is above a certain speed threshold needed for regen braking to be applied. Figure 9 is a detailed description of the vehicle braking system block.

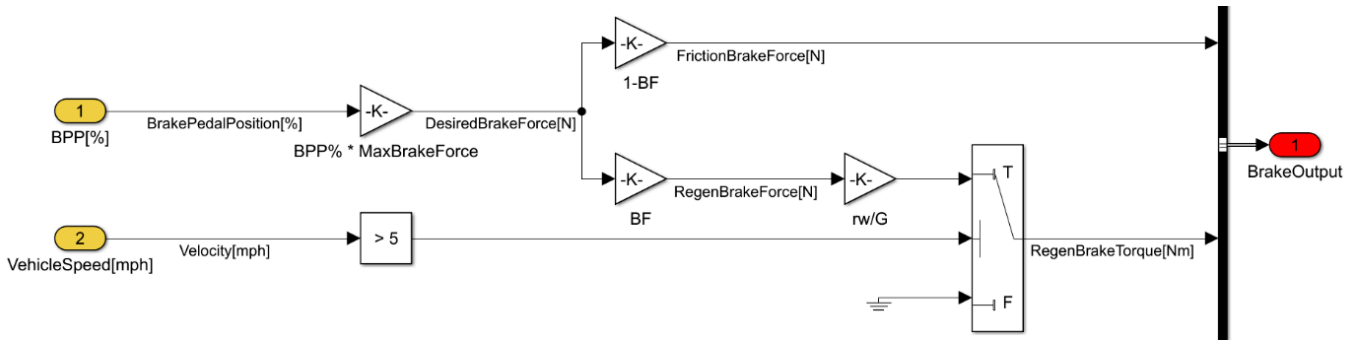

Figure 9. Braking system block Adapted from [16], MathWorks: 2020.

2.7. Motor Model

Electric motors are critical components of the drivetrains of EVs [20]. The electric motor model is based on the power loss equation for electric motors described in Figure 10, where the motor output power is defined by the motor input power minus the motor losses. Table 3 describes the parameter definitions for calculating the motor loss model. The motor model receives an acceleration pedal position signal APP% input and motor speed feedback, these values are then used in the motor torque limiter sub-system described in Figure 11 to determine the max torque output. Similarly, the regen limiter subsystem determines the max allowable regen torque which is a specified by a factor of the maximum allowable torque of the motor. The net torque is then used to calculate the output power using the motor loss model as described by Equations (9)–(11) [16].

$$P_{mot} = T_{mot}\omega_{mot} \tag{9}$$

$$P_{loss} = k_c T^2 + k_i \omega + k_\omega \omega^3 + C \tag{10}$$

$$P_{in} = \tau \times \omega + P_{loss} \tag{11}$$

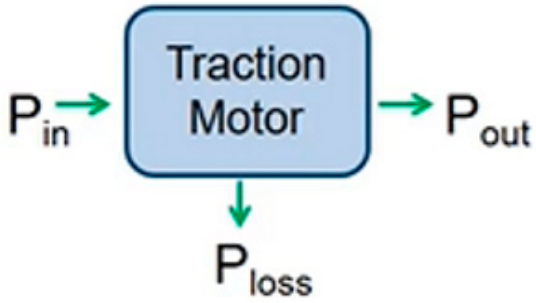

Figure 10. Motor loss model. Adapted from [16], MathWorks: 2020.

Table 3. Motor model parameters. Adapted from [16], MathWorks: 2020.

Parameter	Units	Description	Value
T	Nm	Maximum motor torque	450
ω	rad/s	Motor base speed	834
k_c	$\frac{s}{Kg\ m^2}$	Motor loss constant	0.12
k_i	J	Motor loss constant	0.01
k_w	$Kg\ m^2$	Motor loss constant	1.2×10^{-5}
C	W	Motor loss constant	600

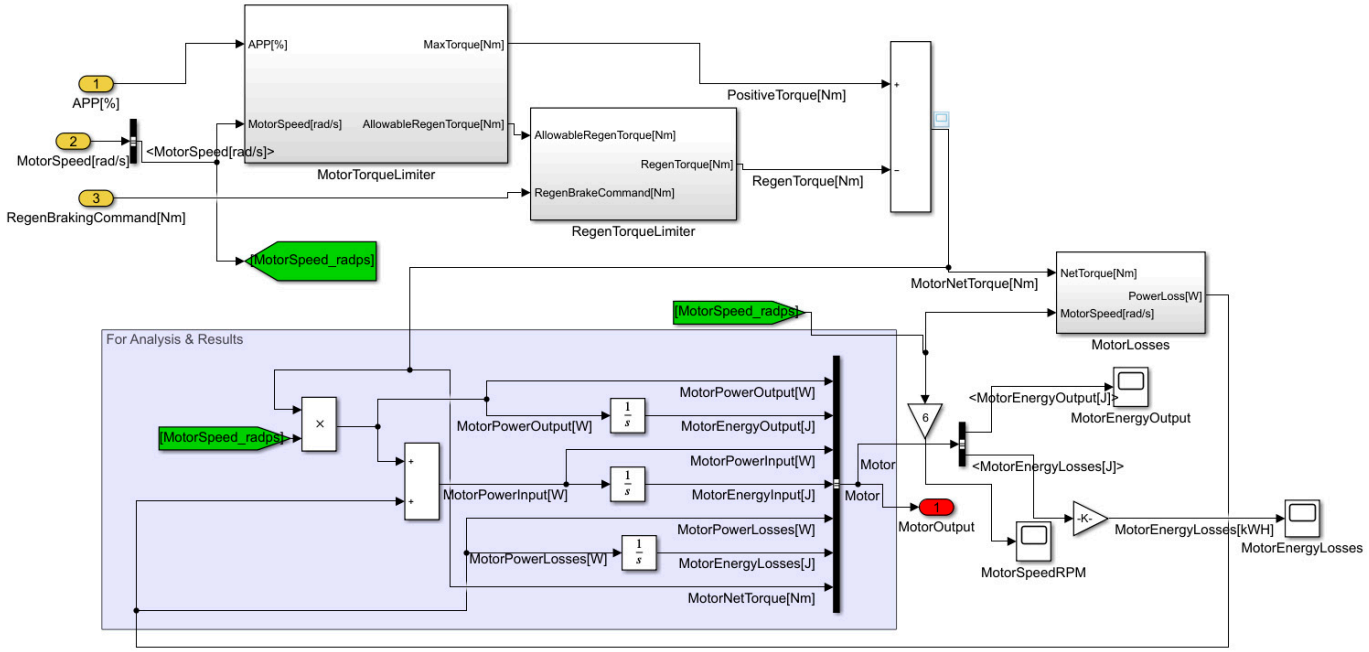

Figure 11. Electric motor model with motor loss model calculations. Adapted from [16], MathWorks: 2020.

2.8. Battery Model

The battery model is developed based off a constant voltage source, V_{oc}, in series with an internal resistance, R_{int} = 0.1 ohms, as described by Figure 12. This model relies on a power loss calculation to determine the battery output current as described by Equations (12)–(15). Figure 13 describes the battery model and loss model calculation in the Simulink Electric Vehicle model [16]. The state of charge (SOC) of the battery is determined by

integrating the power over time and comparing to the energy capacity variable set at the initialization of the simulation.

$$P_{ideal} = P_{actual} + P_{loss} \tag{12}$$

$$P_{ideal} = IV_{oc} \tag{13}$$

$$P_{actual} = IV_{oc} - I^2R_{int} \tag{14}$$

$$P_{loss} = I^2R_{int} \tag{15}$$

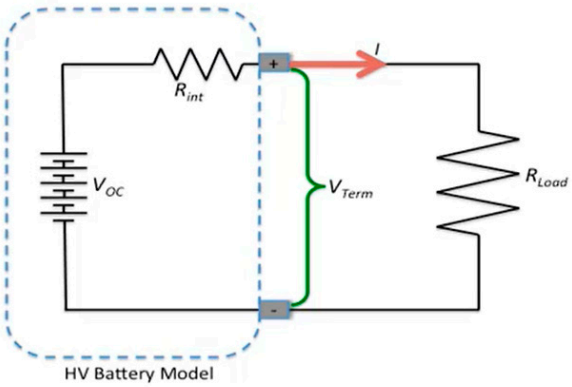

Figure 12. Battery model with internal resistance. Adapted from [16], MathWorks: 2020.

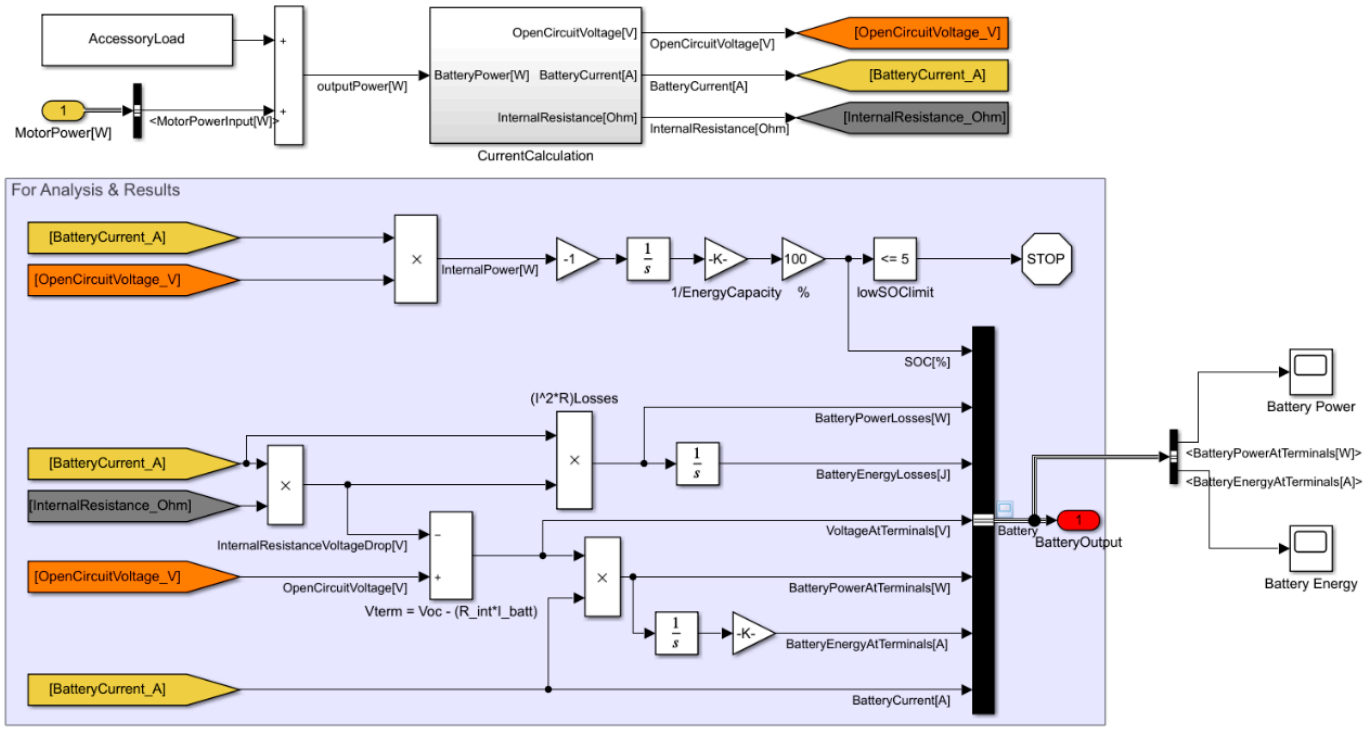

Figure 13. Battery model with SOC and power loss calculations. Adapted from [16], MathWorks: 2020.

2.9. Driveline Model

The driveline model describes the driveline losses that are present in the EV due to gear reduction. The electric motor spins at higher speeds than the wheel and, as a result, gear reduction is used to reduce the speed at the wheel while multiplying the torque at the wheel. This gear reduction is not lossless and is given by T_{loss} in the Equation (16), where

G is the gear ratio of the rear reduction assembly, r_w is the radius of the wheel, F_{tr} in net tractive force at the wheel and F_{Br} is the braking force. Figure 14 is the Simulink model of the driveline and accompanying loss calculations.

$$F_{tr} = \frac{(T_{motor} - T_{loss})G}{r_w} - F_{Br} \tag{16}$$

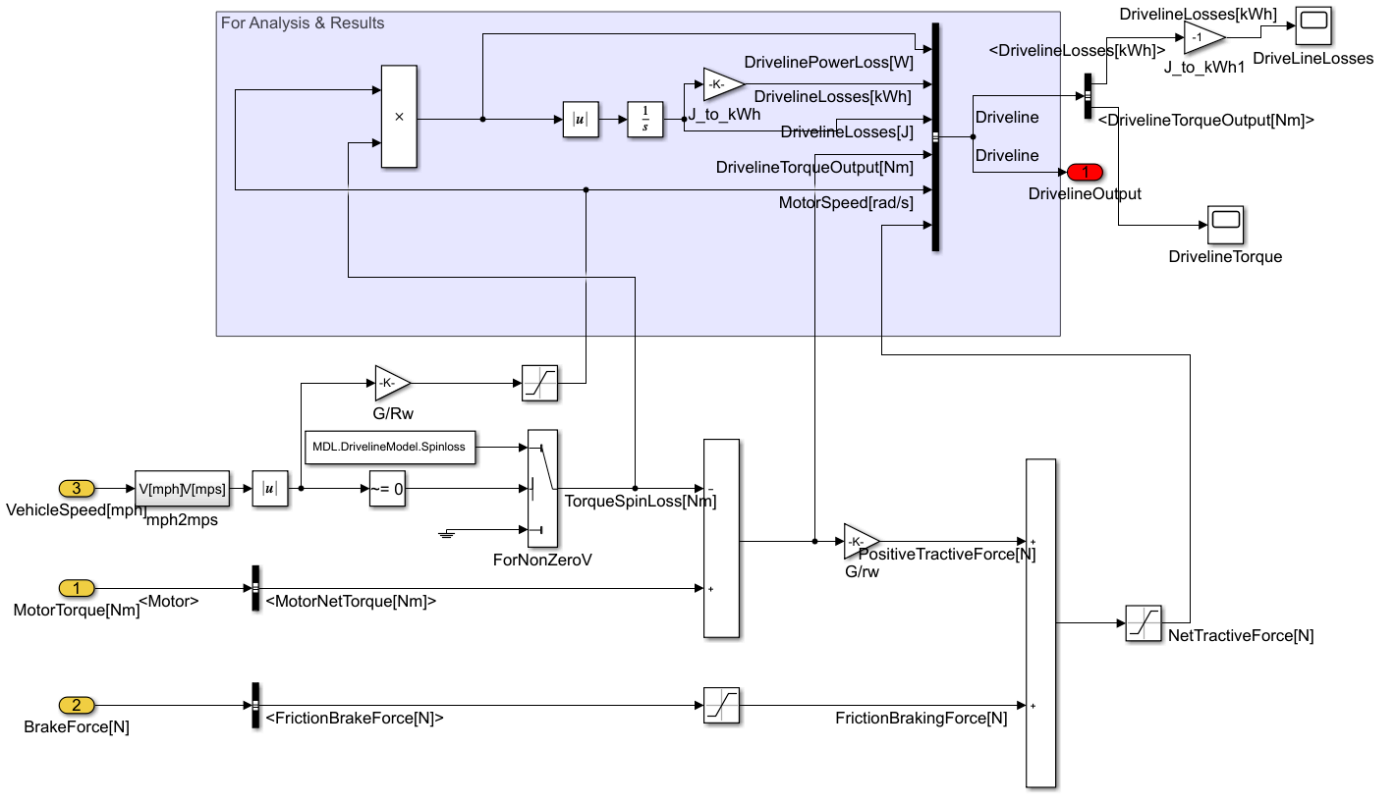

Figure 14. Driveline loss model and calculations Adapted from [16], MathWorks: 2020.

3. EV Chassis Dynamometer Testing

EVs are characterized on a chassis dyno to determine their driving performance [19,21–23]. The vehicle performance testing typically involves driving the vehicle through an EPA drive cycle, such as the MCT drive cycle in Figure 3. Prior to dyno testing of an EV, the dyno must be calibrated to accurately represent the road load forces that are exerted on a vehicle. This involves road load coast down tests, where the vehicle is driven on a flat straight road and accelerating the vehicle to ~60 mph, then shifting the vehicle to neutral gear to remove the regenerative braking capabilities and allowing the vehicle coast down naturally to determine the road load forces acting on vehicle, which include aerodynamic drag and rolling resistance. One such test was conducted in [18] and validated by putting the vehicle through similar drive cycles on the road and the dyno, collecting data through the vehicle on-board diagnostic (OBD) port and then comparing the power and energy of the vehicle over the drive cycles. Figure 15 is a speed plot of the road and dyno tests including the difference in speed between both tests, showing a close correlation between speed over the entire drive cycle. Figure 16 is a plot of the power and energy for both the road and dynamometer tests. Although the dynamic behavior of the vehicle during the road and dyno tests varied, they followed a similar trend over time and the energy consumption was comparable.

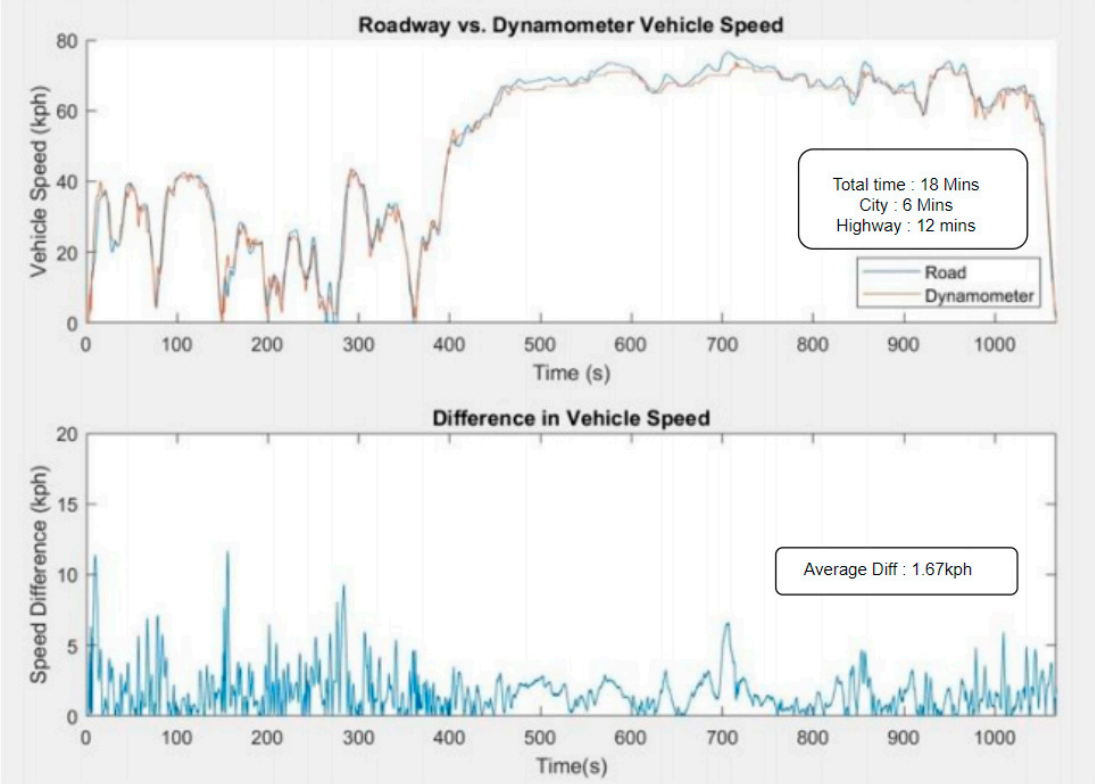

Figure 15. Road and dynamometer test vehicle speed and difference Adapted from [18], IEEE: 2020.

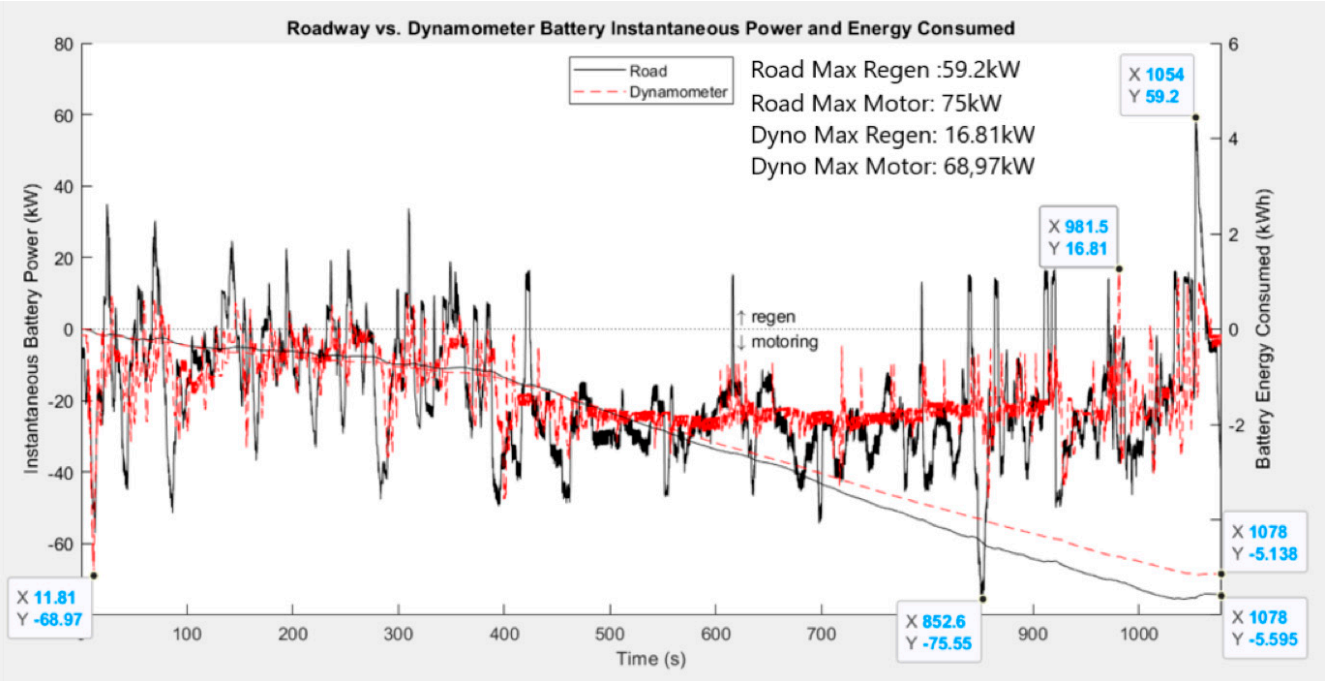

Figure 16. Road and dynamometer test vehicle power (left axis) and energy (right axis). Adapted from [18], IEEE: 2020.

Once the dynamometer was calibrated, the modified MCT test described in Figure 3 was conducted on the vehicle using the dynamometer and the vehicle OBD to instrument the vehicle and collect data for calculating the energy efficiency of the vehicle. Three runs of the same MCT test were carried out on the vehicle and described in Figure 17. The

instantaneous power and energy of each cycle was recorded during the drive cycles and summarized in Figure 18. Finally, a vehicle acceleration performance test, known as the wide-open throttle (WOT) test, was conducted on the vehicle to determine the vehicle initial acceleration capability described in Figure 19. The dynamometer tests resulted in an energy efficiency average of 297 Wh/mile and an initial acceleration of 7.5 s from 0–60 mph (96.44 kph).

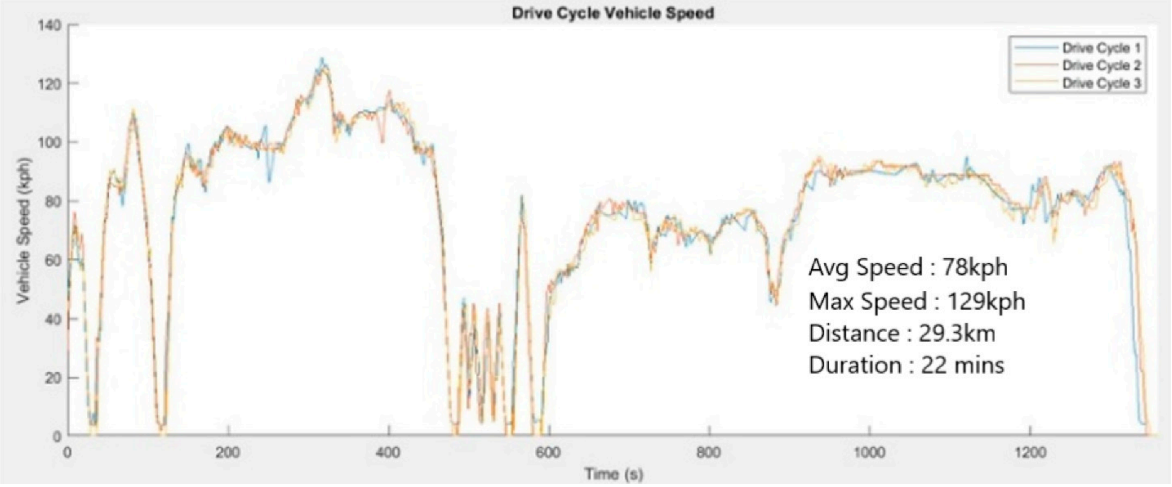

Figure 17. MCT drive cycle vehicle speed on chassis dynamometer Adapted from [18], IEEE: 2020.

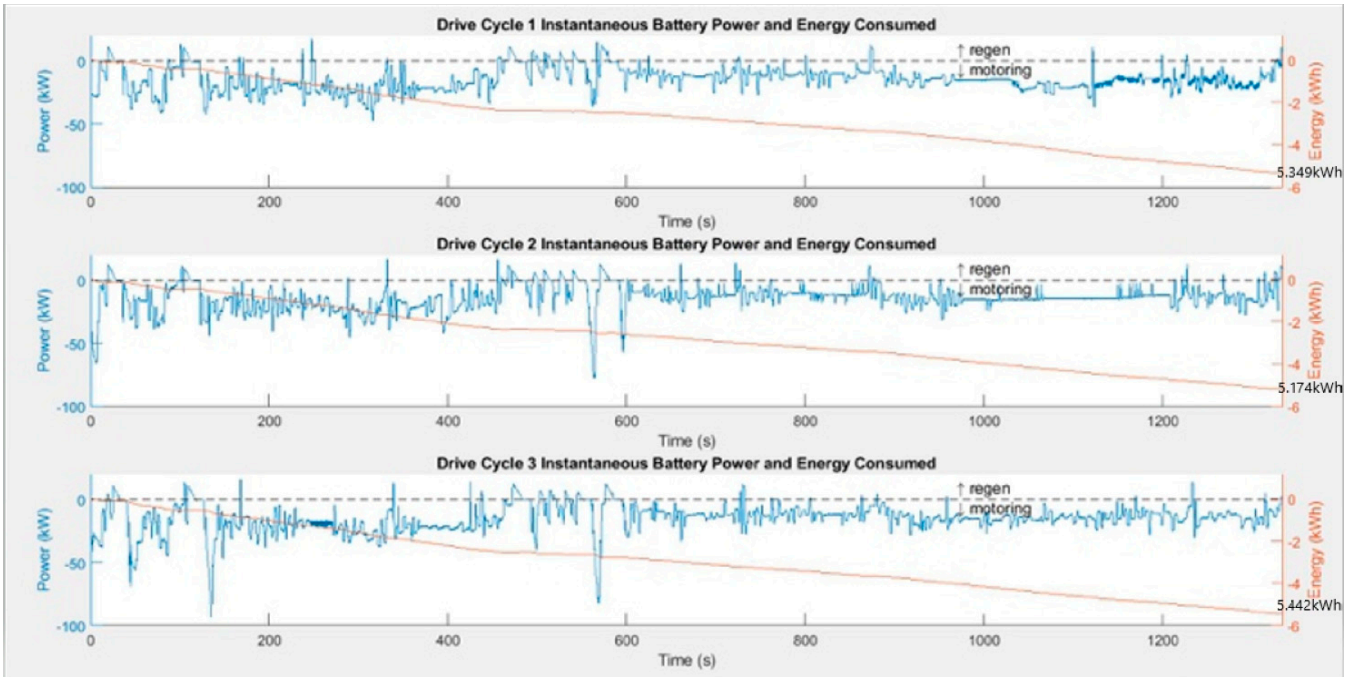

Figure 18. MCT drive cycle vehicle power (left axis) and energy (right axis) on chassis dynamometer Adapted from [18], IEEE: 2020.

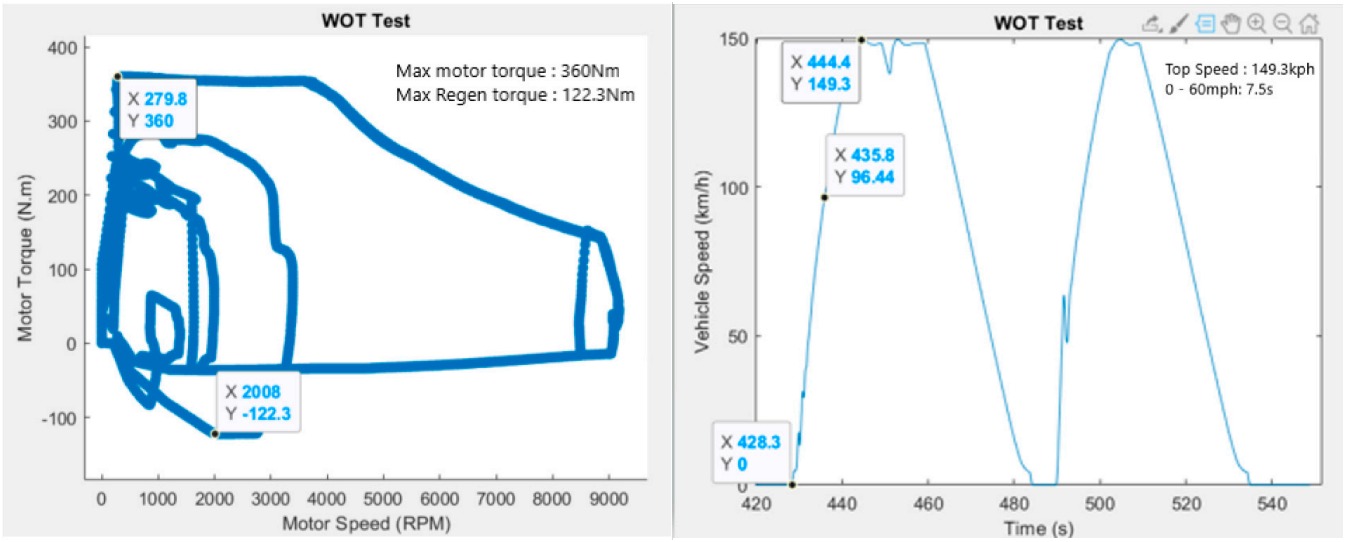

(**a**) (**b**)

Figure 19. Wide-open throttle (WOT) test (**a**) motor torque envelope (**b**) vehicle speed Adapted from [18], IEEE: 2020.

The WOT test showed the vehicle was capable of attaining a top of speed of 93 mph, while almost instantly reaching the maximum torque treshold of 360 Nm as indicated in Figure 19. In Summary, the EV chassis dynamometer results serve as a strong basis for validating the results of a vehicle model developed and simulated within a software environment through an iterative design process. The controlled test environment of using a chassis dyno to emulate road load forces allows for ease and repeatability of testing cycles during the vehicle development and vaidation stages. The real-world driving use cases emulated on the dyno can then be validated in the sofware simulation environment and vice versa. Although slight error and deviations can be observed in dyno vs. road tests as indicated in Figures 15 and 16, these errors are negligible in most cases, however, it is difficult and sometimes unsafe to perform some of the rigourous vehicle driving scenerios needed for testing high performace vehicles on public roads. The next section presents detailed results and analysis of the dyno test results and the simulations results.

4. Validation of EV Model Simulation Results and Analysis

Given the high repeatability of the chassis dynamometer testing, the EV model developed above was then validated against the dyno work, with careful comparison of the observations, including speed, distance, energy expended and power between modeling, chassis dynamometer, and on-road measurements. It is important to note that due to the advanced dynamics controls on the real vehicle in comparison to the simplified PID controls modeled, the dynamic responses of the modeled vehicle and the real vehicle, such as motor torque and power, are expected to vary to a certain degree. However, the steady state values, such as speed, distance and energy, do show a strong correlation.

Figure 20 is a plot of the vehicle speed during the simulation overlayed on the drive cycle speed, which was recorded via the OBD port during dyno testing. From the plot in Figure 20, we observe that the modeled vehicle is capable of following the drive cycle input closely within a very small margin of error while meeting the speed and torque response requirements. Figure 21 is a plot of the battery SOC over the drive cycle period. The model was initialized to 95% SOC at the beginning of the model and ended at 85% at the end of the simulation. Recall that the modeled vehicle battery total capacity 53 kWh, indicating that ~10% of the battery total capacity was depleted during the drive cycle.

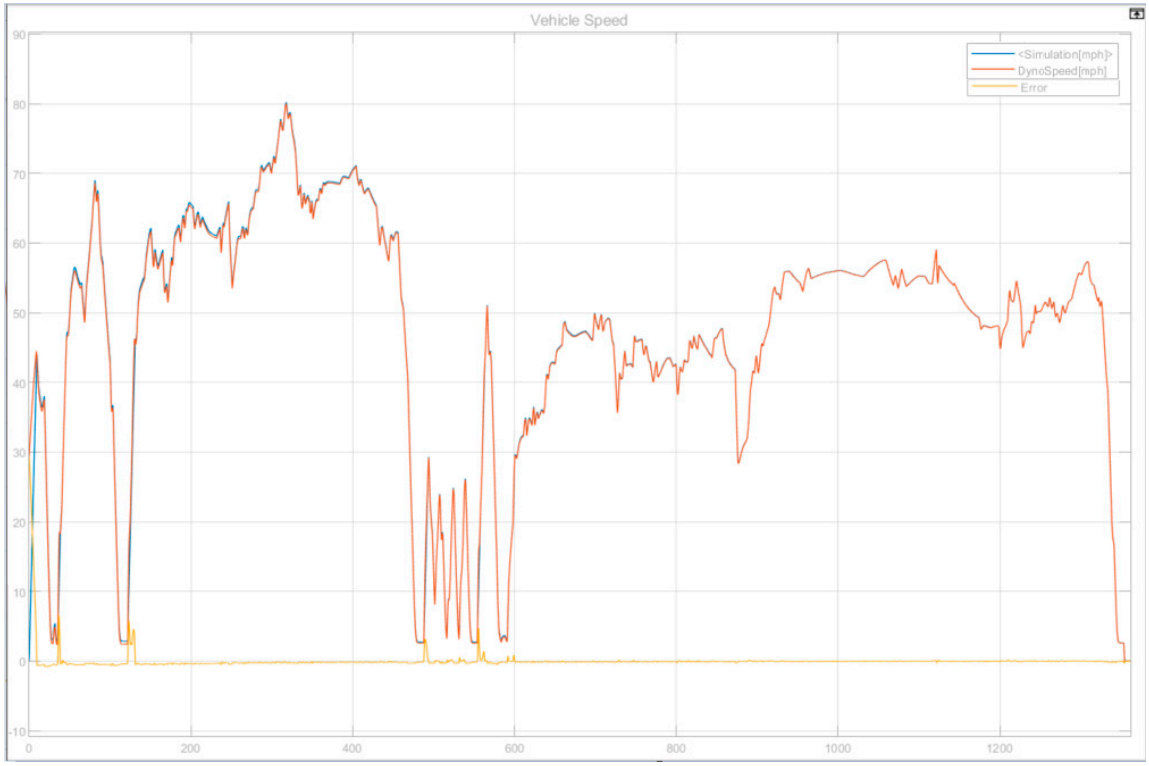

Figure 20. Modeled vehicle speed (mph) over time (secs) compared to dyno drive cycle speed.

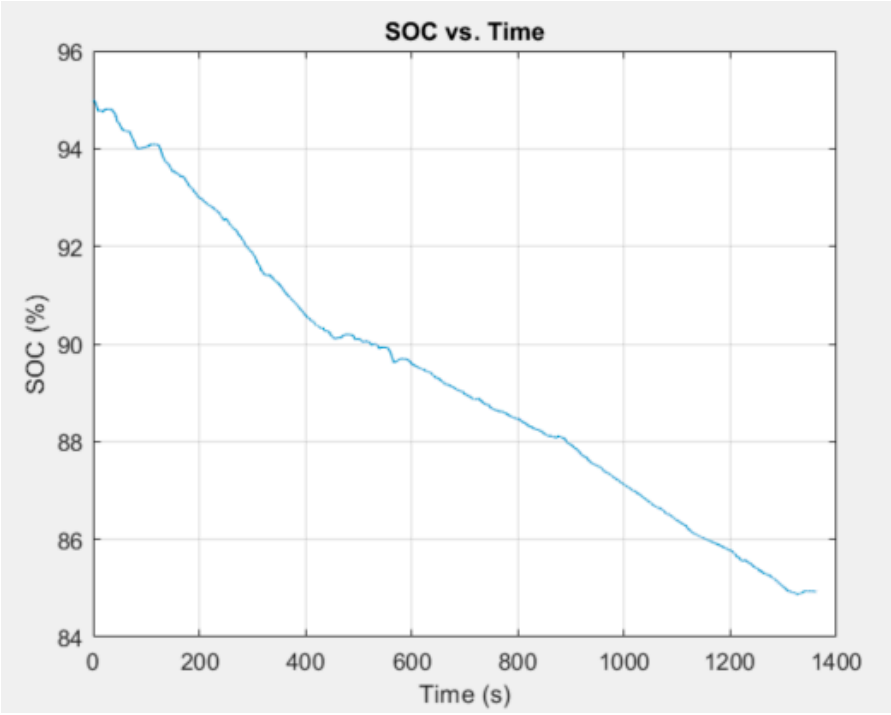

Figure 21. Modeled battery SOC over time.

Figure 22 is a plot comparison of the battery energy over time between the dyno test and vehicle simulation, which is derived by integrating the battery power over time, as seen in the model block diagrams in Figure 13. Figure 23 is a plot comparison of the vehicle distance over time, which is an integration of the vehicle speed over time.

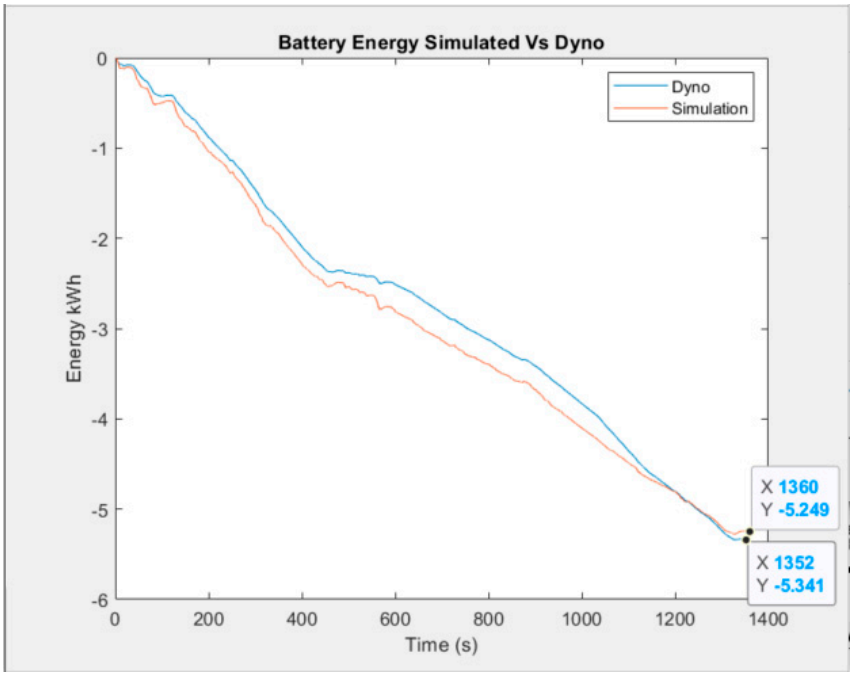

Figure 22. Battery energy over time.

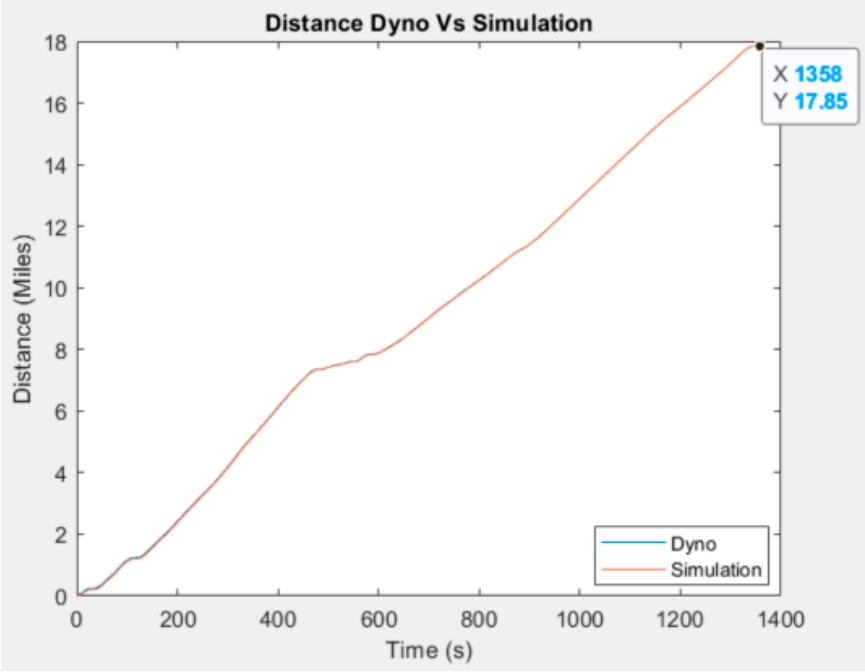

Figure 23. Vehicle distance covered over time.

4.1. Energy Efficiency

The energy efficiency of the modeled EV can be derived by the dividing the battery energy output by the vehicle distance covered. The total energy delivered by the battery model was 5.249 kWh, while the distance traveled was 17.85 miles, which resulted in an energy efficiency of 294 Wh/mile compared to the dynamometer tests results, which had an overall energy efficiency average of 297 Wh/mile. The root-mean-square error (RMSE) between the modeled EV results and the dyno results was calculated for a final value of 0.2 for measured energy consumption over time. The small error deviations in the model can be attributed to negligible transient errors within the model.

4.2. Motor Torque and Power

Figure 24 is a plot of the vehicle power over the vehicle speed range, indicating the power regions the motor operated over the drive cycle. From the plot, we can determine the vehicle model rated speed is around 40 mph, and then, between 40 mph to 70 mph, the vehicle is in the constant power region, with a concentration of motor operating points in this region. The diagonal line in the power plot is attributed to the initial acceleration of the vehicle from 0 mph to ~40 mph at the very beginning of the drive cycle and towards the 600 s mark. Figure 25 is a scatter plot of motor torque over the vehicle speed change from the simulated drive cycle and the dyno test. From these plots, we draw similarities between the two plots, where the maximum torque (simulation) and the peak torque (dyno) occur between 0 and 40 mph speed range, the constant torque region, and then the gradual ramp down in torque as the speed increases. Similar to the observations in Figure 24, there is a concentration in operating point between 40 mph to 70 mph in both plots, which is consistent with the drive cycle speeds in Figure 20. There is however a significant difference in the dynamic behavior of the dyno motor torque compared to the simulation that can be attributed to the sophisticated motor control schemes implemented in the real vehicle compared to the simplified PID controller that is modeled. These sophisticated controls are implemented in the real-world vehicle to allow for ease of drivability and responsiveness of the vehicle. For example, in the dyno torque plots, we observed a continuity in the torque values at all times without sudden jumps or drops in torque value as speed changes compared to the simulated torque -speed plots. This is due to the effective and careful avoidance of torque ripples by the motor controller implemented on the real-world vehicle. The simulated vehicle model's torque controls calculate the maximum torque based on current vehicle speed and the requested APP% at each time step. A more advanced model will take into consideration the dynamic response of the vehicle and simulate a smoother transition in torque applied, similar to the dyno vehicle response. The expected torque envelope regions of the torque plots captures the expected torque-speed envelope however, showing an attainment of maximum traction and regen torque at lower speeds and reduced torque at higher speeds, as indicated in the torque over time plots in Figure 26 as well.

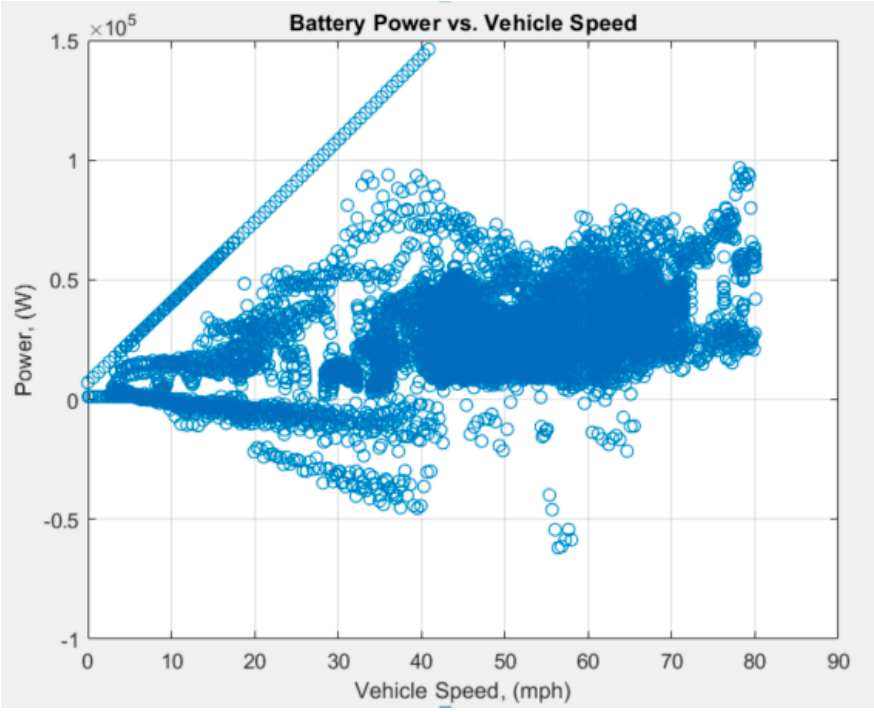

Figure 24. Motor power vs. speed for MCT drive cycle simulation.

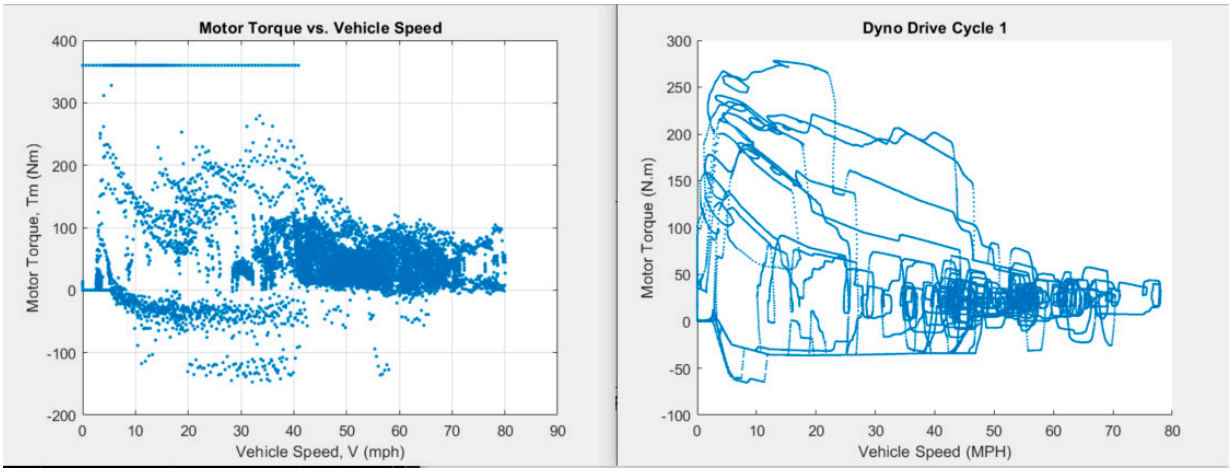

(**a**) Simulation (**b**) Dyno

Figure 25. Motor torque vs. speed (**a**) simulation (**b**) dyno test.

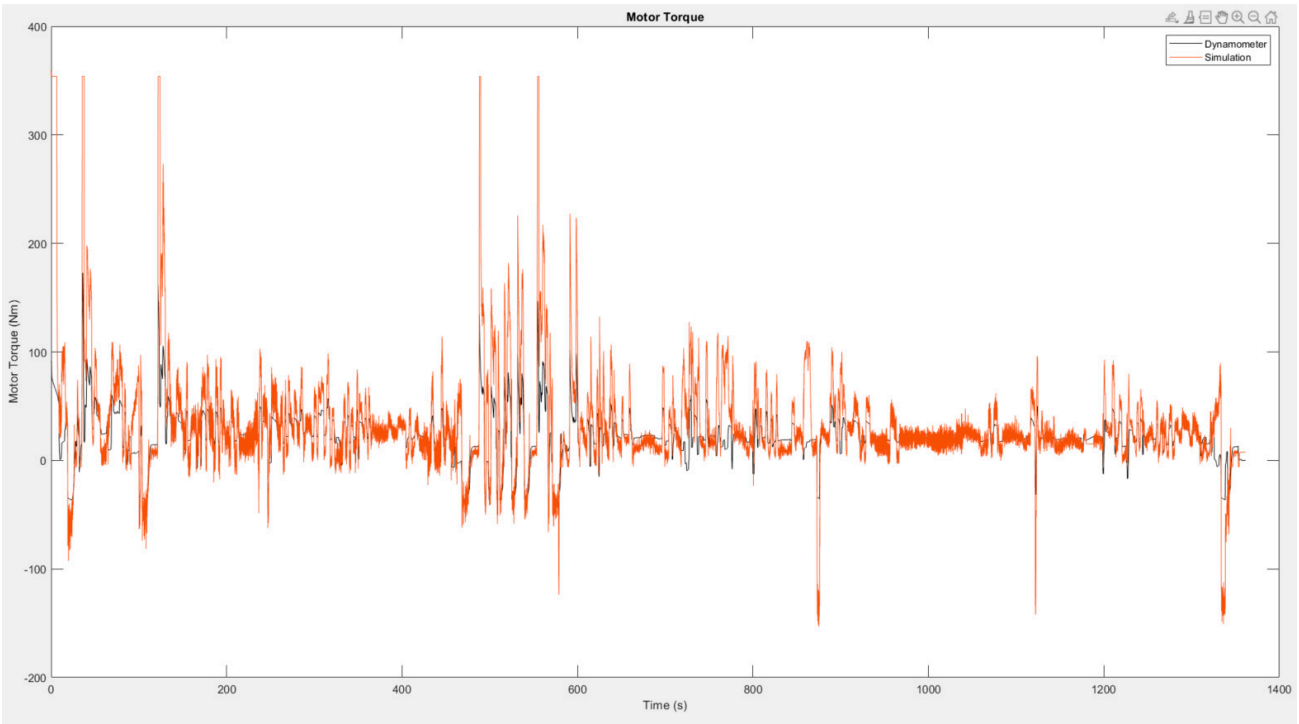

Figure 26. Motor torque vs. time plot.

4.3. Loss Model

The battery energy at the battery terminal is 5.229 kWh as indicated in Figure 22 and is consistent with the energy consumption during dyno testing. The total tractive energy consumption of the vehicle over the drive cycle is measured at 3.18 kWh as indicated in Figure 27, while the motor energy losses are measured at 0.71 kWh as indicated in Figure 28, and the driveline losses From Figure 29 are measured at 0.5 kWh, indicating that the total energy used to overcome the road load forces acting on the vehicle, F_{RL}, is 0.839 kWh. Although Figure 22 validated the total energy comsumption correlation of the model to the dyno, the figures below allow us to estimate, experiment and validate the efficiency of the real-world vehicle compared to the vehicle model. The vehicle model can

be optimized iteratively to reduce these losses through either reduction in motor losses by adjusting the motors operational limits or modifying the driveline gear selection.

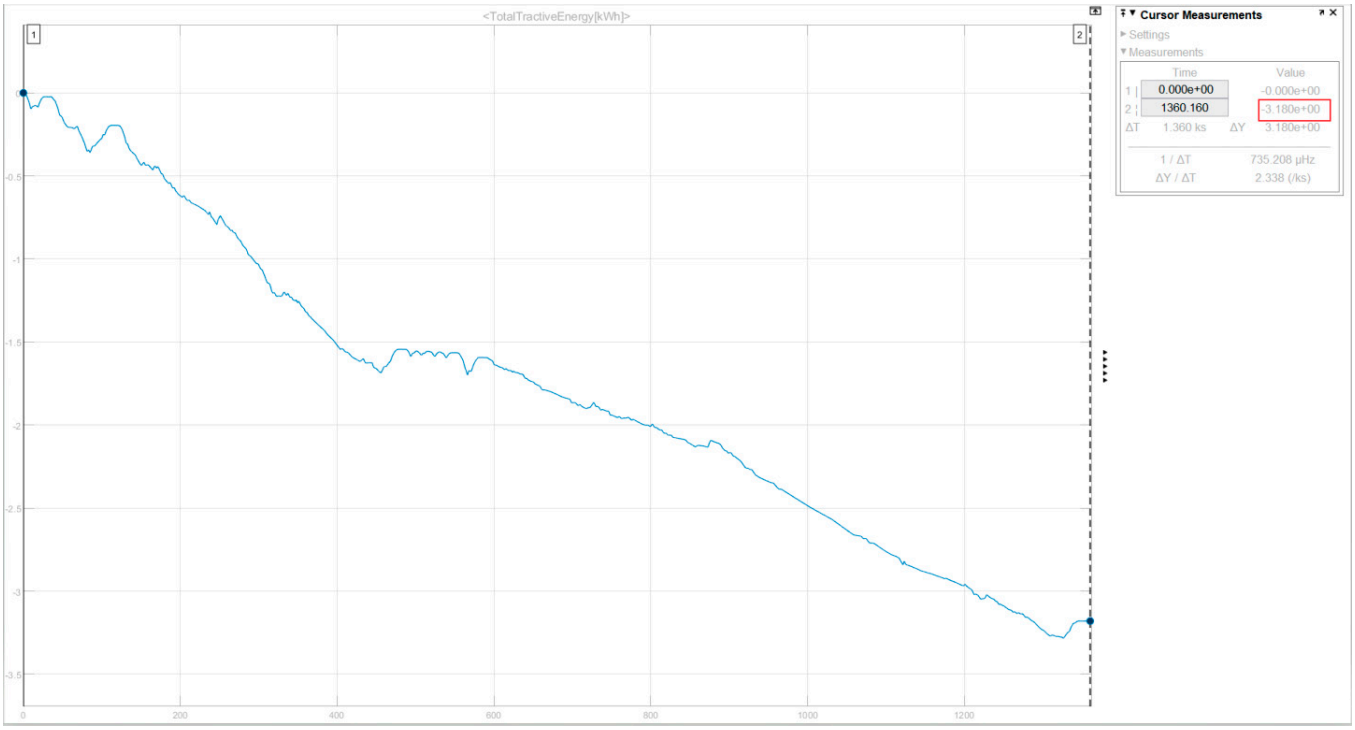

Figure 27. Vehicle tractive energy over time.

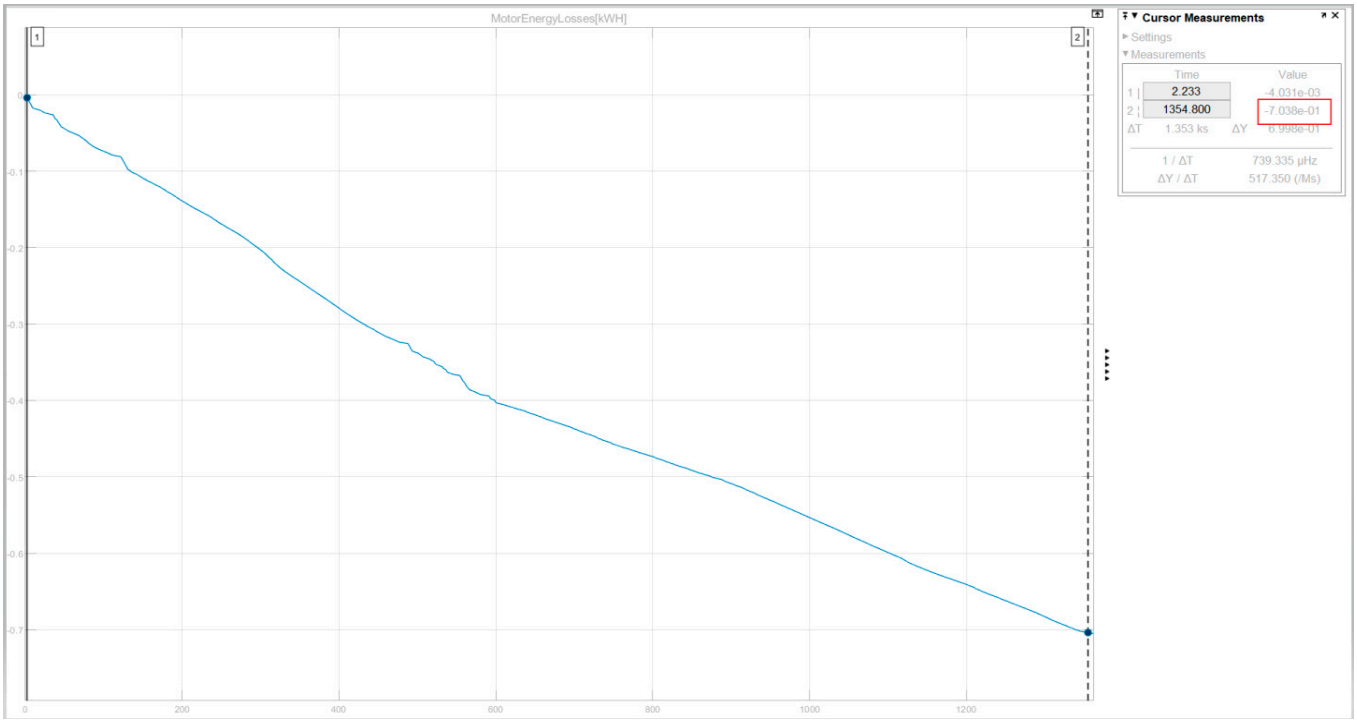

Figure 28. Motor energy losses over time.

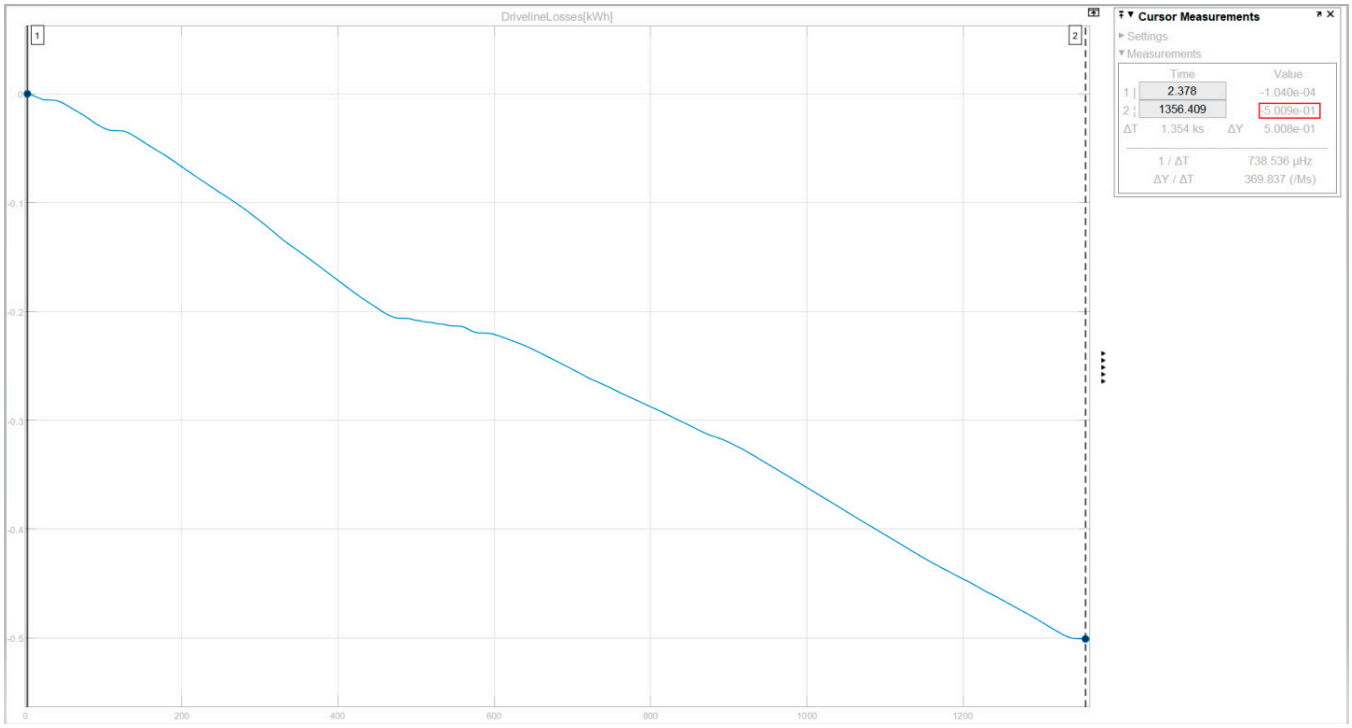

Figure 29. Driveline energy losses over time.

5. Conclusions

This paper highlights the importance of high performance EV modeling, simulation, and validation due to the revolutionization of the transportation industry by electric mobility. The objective of this work was to demonstrate the methodologies for developing high performance EV models in a software simulation environment and validating the models with real-world hardware in a repeatable and scalable fashion, thereby enabling the rapid development of EV testbeds. A brief review of EV modeling techniques and software toolsets were introduced. A summary of EV motion dynamics was described mathematically and an equation based EV model was implemented based on the mathematical models described. The design philosophy of EV OEMs with regard to vehicle efficiency drive cycle tests mandated by the EPA were briefly described. Finally, the results of the EV model were validated by comparing them to the results of vehicle performance tests of the specified EV on a chassis dynamometer. The energy efficiency results of the modeled high performance EV compared to the real-world vehicle showed close correlation with a root-mean-square error (RMSE) value of 0.2. The vehicle speed and vehicle distance traveled of the model also resulted in negligible error values. The modeled motor control strategies, however, did not capture the dynamic and transient behavior of the real-world vehicle adequately. Although the equation-based model provided a valuable means of gaining an understanding of the how the modeled vehicle will perform under certain driving conditions from an energy efficiency standpoint, this modeling approach is not suitable for detailed analysis of vehicle dynamics and evaluation of control strategies. Future work will consider a physical modeling approach which enables the development of an advanced motor model such as data driven/map based motor models, and advanced motor controller schemes such as six-step control or space vector modulation (SVM) controls which should result in more detailed and accurate transient and dynamic responses compared to the real-world vehicle. A physical modeling approach would also include more advanced battery models that consider the thermal relationship between individual cells within a pack and ambient temperature conditions, as well as degradation mechanisms that affect state of power (SOP) and state of health (SOH) during drive cycles simulations.

Author Contributions: Conceptualization, F.A.; methodology, F.A. and A.v.J.; validation, F.A., A.v.J., A.Y., B.P. and E.A.; formal analysis, F.A.; investigation, F.A., A.v.J. and A.Y.; data curation, F.A.; writing—original draft preparation, F.A.; writing—review and editing, F.A., A.v.J., A.Y., B.P. and E.A.; supervision, A.v.J., A.Y.; project administration, A.v.J. All authors have read and agreed to the published version of the manuscript.

Funding: This research received no external funding.

Institutional Review Board Statement: Not applicable.

Informed Consent Statement: Not applicable.

Data Availability Statement: Not applicable.

Conflicts of Interest: The authors declare no conflict of interest.

References

1. BNEF. *EV Sales 2020*; Bloomberg New Energy Finance: New York, NY, USA, 2020.
2. IEA. *Global EV Outlook 2019*; International Energy Agency: Paris, France, 2019.
3. Kumar, R.R.; Alok, K. Adoption of electric vehicle: A literature review and prospects for sustainability. *J. Clean. Prod.* **2020**, *253*, 119911. [CrossRef]
4. Traffic Safety Facts. *2016 Fatal Motor Vehicle Crashes: Overview*; Research Note DOT HS 812 456; U.S. Department of Transportation, NHTSA's National Center for Statistics and Analysis: Washington, DC, USA, 2017.
5. Rowley, J.; Liu, A.; Sandry, S.; Gross, J.; Salvador, M.; Anton, C.; Fleming, C. Examining the driverless future: An analysis of human-caused vehicle accidents and development of an autonomous vehicle communication testbed. In Proceedings of the IEEE Systems and Information Engineering Design Symposium (SIEDS), Charlottesville, VA, USA, 27 April 2018.
6. Kricke, C.; Hagel, S. A hybrid electric vehicle simulation model for component design and energy management optimization. In Proceedings of the FISITA World Automotive Congress, Paris, France, 27 September–1 October 1998.
7. Auert, B.; Cheny, C.; Raison, B.; Berthon, A. Software tool for the simulation of the electro- mechanical behavior of a hybrid vehicle. In Proceedings of the Electric Vehicle Symposium 15, Brussels, Belgium, 29 September–3 October 1998.
8. Onoda, S.; Emadi, A. PSIM-Based Modeling of Automotive Power Systems: Conventional, Electric, and Hybrid Electric Vehicles. *IEEE Trans. Veh. Technol.* **2004**, *53*, 390–400. [CrossRef]
9. Amrhein, M.; Krein, P.T. Dynamic Simulation for Analysis of Hybrid Electric Vehicle System and Subsystem Interactions, Including Power Electronics. *IEEE Trans. Veh. Technol.* **2005**, *54*, 825–836. [CrossRef]
10. Baisden, A.C.; Emadi, A. An ADVISOR based mode of a battery and an ultra-capacitor energy source for hybrid electric vehicles. *IEEE Trans. Veh. Technol.* **2004**, *53*, 199–205. [CrossRef]
11. Gao, D.W.; Mi, C.; Emadi, A. Modeling and Simulation of Electric and Hybrid Vehicles. *Proc. IEEE* **2007**, *95*, 729–745. [CrossRef]
12. Alam Chowdhury, M.S.; Al Mamun, K.A.; Rahman, A.M. Modelling and simulation of power system of battery, solar and fuel cell powered Hybrid Electric vehicle. In Proceedings of the 2016 3rd International Conference on Electrical Engineering and Information Communication Technology, Dhaka, Bangladesh, 22–24 September 2016; pp. 1–6. [CrossRef]
13. Yaich, M.; Hachicha, M.R.; Ghariani, M. Modeling and simulation of electric and hybrid vehicles for recreational vehicle. In Proceedings of the 2015 16th International Conference on Sciences and Techniques of Automatic Control and Computer Engineering (STA), Monastir, Tunisia, 21–23 December 2015; pp. 181–187. [CrossRef]
14. Zhou, J.; Shen, X.; Liu, D. Modeling and simulation for electric vehicle powertrain controls. In Proceedings of the 2014 IEEE Conference and Expo Transportation Electrification Asia-Pacific (ITEC Asia-Pacific), Beijing, China, 31 August–3 September 2014; pp. 1–4. [CrossRef]
15. Tremblay, O.; Dessaint, L.; Dekkiche, A. A Generic Battery Model for the Dynamic Simulation of Hybrid Electric Vehicles. In Proceedings of the 2007 IEEE Vehicle Power and Propulsion Conference, Arlington, TX, USA, 9–12 September 2007; pp. 284–289. [CrossRef]
16. MathWorks Student Competitions Team 2021. MATLAB and Simulink Racing Lounge: Vehicle Modeling. GitHub. Available online: https://github.com/mathworks/vehicle-modeling/releases/tag/v4.1.1 (accessed on 10 January 2021).
17. Husain, I. *Electric and Hybrid Vehicles: Design Fundamentals*, 2nd ed.; CRC Press LLC: Boca Raton, FL, USA, 2010.
18. Von Jouanne, A.; Adegbohun, J.; Collin, R.; Stephens, M.; Thayil, B.; Li, C.; Agamloh, E.; Yokochi, A. Electric Vehicle (EV) Chassis Dynamometer Testing. In Proceedings of the 2020 IEEE Energy Conversion Congress and Exposition (ECCE), Detroit, MI, USA, 11–15 October 2020; pp. 897–904. [CrossRef]
19. SAE International. *J1634 in Battery Electric Vehicle Energy Consumption and Range Test Procedure*; SAE International: Warrendale, PA, USA, 2017.
20. Agamloh, E.; Von Jouanne, A.; Yokochi, A. An Overview of Electric Machine Trends in Modern Electric Vehicles. *Machines* **2020**, *8*, 20. [CrossRef]
21. Schauer, J.J.; Kleeman, M.J.; Cass, G.R.; Simoneit, B.R.T. Measurement of Emissions from Air Pollution Sources. 2. C1through C30Organic Compounds from Medium Duty Diesel Trucks. *Environ. Sci. Technol.* **1999**, *33*, 1578–1587. [CrossRef]

22. Zielinska, B.; Sagebiel, J.; McDonald, J.D.; Whitney, K.; Lawson, D.R. Emission Rates and Comparative Chemical Composition from Selected In-Use Diesel and Gasoline-Fueled Vehicles. *J. Air Waste Manag. Assoc.* **2004**, *54*, 1138–1150. [CrossRef] [PubMed]
23. Kogelschatz, U. Dielectric-barrier Discharges: Their History, Discharge Physics, and Industrial Applications. *Plasma Chem. Plasma Proc.* **2003**, *23*, 1–46. [CrossRef]